

# Fundamental limits on the rate of bacterial cell division

**Nathan M. Belliveau<sup>†, 1</sup>, Griffin Chure<sup>†, 2, 3</sup>, Christina L. Hueschen<sup>4</sup>, Hernan G. Garcia<sup>5</sup>, Jané Kondev<sup>6</sup>, Daniel S. Fisher<sup>7</sup>, Julie Theriot<sup>1, 8</sup>, Rob Phillips<sup>2, 9,\*</sup>**

\*For correspondence:

<sup>†</sup>These authors contributed equally to this work

<sup>1</sup>Department of Biology, University of Washington, Seattle, WA, USA; <sup>2</sup>Division of Biology and Biological Engineering, California Institute of Technology, Pasadena, CA, USA; <sup>3</sup>Department of Applied Physics, California Institute of Technology, Pasadena, CA, USA; <sup>4</sup>Department of Chemical Engineering, Stanford University, Stanford, CA, USA; <sup>5</sup>Department of Molecular Cell Biology and Department of Physics, University of California Berkeley, Berkeley, CA, USA; <sup>6</sup>Department of Physics, Brandeis University, Waltham, MA, USA; <sup>7</sup>Department of Applied Physics, Stanford University, Stanford, CA, USA; <sup>8</sup>Allen Institute for Cell Science, Seattle, WA, USA; <sup>9</sup>Department of Physics, California Institute of Technology, Pasadena, CA, USA; \*Contributed equally

## Abstract

## Introduction

The range of bacterial growth rates is enormously diverse. In natural environments, some microbial organisms might double only once per year while in comfortable laboratory conditions, growth can be rapid with several divisions per hour. This six order of magnitude difference illustrates the intimate relationship between environmental conditions and the rates at which cells convert nutrients into new cellular material – a relationship that has remained a major topic of inquiry in bacterial physiology for over a century (*Jun et al., 2018*). As was noted by Jacques Monod, “the study of the growth of bacterial cultures does not constitute a specialized subject or branch of research, it is the basic method of Microbiology.” Those words ring as true today as they did when they were written 70 years ago. Indeed, the study of bacterial growth has undergone a molecular resurgence since many of the key questions addressed by the pioneering efforts in the middle of the last century can be revisited by examining them through the lens of the increasingly refined molecular census that is available for bacteria such as the microbial workhorse *Escherichia coli*. Several of the outstanding questions that can now be studied about bacterial growth include: what sets the fastest time scale that bacteria can divide, and how is growth rate tied to the quality of the carbon source. In this paper, we address these two questions from two distinct angles. First, as a result of an array of high-quality proteome-wide measurements of the *E. coli* proteome under a myriad of different growth conditions, we have a census that allows us to explore how the number of key molecular players change as a function of growth rate. This census provides a window onto whether the processes they mediate such as molecular transport into the cells and molecular synthesis within cells can run faster. Second, because of our understanding of the molecular pathways responsible for many of the steps in bacterial growth, we can also make order of magnitude estimates to infer the copy numbers that would be needed to achieve a given growth rate. In this paper, we pass back and forth between the analysis of a variety of different proteomic datasets and order-of-magnitude estimations to determine possible molecular bottlenecks that limit bacterial growth and to see how

42 the growth rate varies in different carbon sources.

43 Specifically, we leverage a combination of *E. coli* proteomic data sets collected over the past  
 44 decade using either mass spectrometry (*Schmidt et al., 2016; Peebo et al., 2015; Valgepea et al.,*  
 45 **2013**) or ribosomal profiling (*Li et al., 2014*) across 31 unique growth conditions. Broadly speaking,  
 46 we entertain several classes of hypotheses as are illustrated in **Figure 1**. First, we consider potential  
 47 limits on the transport of nutrients into the cell. We address this hypothesis by performing an  
 48 order-of-magnitude estimate for how many carbon, phosphorous, and sulfur atoms are needed to  
 49 facilitate this requirement given a 5000 second division time. As a second hypothesis, we consider  
 50 the possibility that there exists a fundamental limit on how quickly the cell can generate ATP. We  
 51 approach this hypothesis from two angles, considering how many ATP synthase complexes must  
 52 be needed to churn out enough ATP to power protein translation followed by an estimation of  
 53 how many electron transport complexes must be present to maintain the proton motive force.  
 54 A third class of estimates considers the need to maintain the size and shape of the cell through  
 55 the construction of new lipids for the cell membranes as well as the glycan polymers which make  
 56 up the rigid peptidoglycan. Our final class of hypotheses centers on the synthesis of a variety of  
 57 biomolecules. Our focus is primarily on the stages of the central dogma as we estimate the number  
 58 of protein complexes needed for DNA replication, transcription, and protein translation.

59 In broad terms, we find that the majority of these estimates are in close agreement with the  
 60 experimental observations, with protein copy numbers apparently well-tuned for the task of cell  
 61 doubling. This allows us to systematically scratch off the hypotheses diagrammed in **Figure 1** as  
 62 setting possible speed limits. Ultimately, we find that protein translation (particularly the generation  
 63 of new ribosomes) acts as 1) a rate limiting step for the *fastest* bacterial division, and 2) the major  
 64 determinant of bacterial growth across all nutrient conditions we have considered under steady  
 65 state, exponential growth. This perspective is in line with the linear correlation observed between  
 66 growth rate and ribosomal content (typically quantified through the ratio of RNA to protein) for fast  
 67 growing cells (*Scott et al., 2010*), but suggests a more prominent role for ribosomes in setting the  
 68 doubling time across all conditions of nutrient limitation. Here we again leverage the quantitative  
 69 nature of this data set and present a quantitative model of the relationship between the fraction of  
 70 the proteome devoted to ribosomes and the speed limit of translation, revealing a fundamental  
 71 tradeoff between the translation capacity of the ribosome pool and the maximal growth rate.

## 72 Uptake of Nutrients

73 In order to build new cellular mass, the molecular and elemental building blocks must be scavenged  
 74 from the environment in different forms. Carbon, for example, is acquired via the transport of  
 75 carbohydrates and sugar alcohols with some carbon sources receiving preferential treatment  
 76 in their consumption (*Monod, 1947*). Phosphorus, sulfur, and nitrogen, on the other hand, are  
 77 harvested primarily in the forms of inorganic salts, namely phosphate, sulfate, and ammonia  
 78 (*Jun et al., 2018; Assentoft et al., 2016; Stasi et al., 2019; Antonenko et al., 1997; Rosenberg et al.,*  
 79 **1977; Willsky et al., 1973**). All of these compounds have different permeabilities across the cell  
 80 membrane and most require some energetic investment either via ATP hydrolysis or through the  
 81 proton electrochemical gradient to bring the material across the hydrophobic cell membrane. Given  
 82 the diversity of biological transport mechanisms and the vast number of inputs needed to build a  
 83 cell, we begin by considering transport of some of the most important cellular ingredients: carbon,  
 84 nitrogen, oxygen, hydrogen, phosphorus, and sulfur.

85 The elemental composition of *E. coli* has received much quantitative attention over the past  
 86 half century (*Neidhardt et al., 1991; Taymaz-Nikerel et al., 2010; Heldal et al., 1985; Bauer and Ziv,*  
 87 **1976**), providing us with a starting point for estimating the copy numbers of various transporters.  
 88 While there is some variability in the exact elemental percentages (with different uncertainties), we  
 89 can estimate that the dry mass of a typical *E. coli* cell is  $\approx$  45% carbon (BNID: 100649, *Milo et al.*  
 90 **(2010)**),  $\approx$  15% nitrogen (BNID: 106666, *Milo et al. (2010)*),  $\approx$  3% phosphorus (BNID: 100653, *Milo*  
 91 **et al. (2010)**), and 1% sulfur (BNID: 100655, *Milo et al. (2010)*). In the coming paragraphs, we will

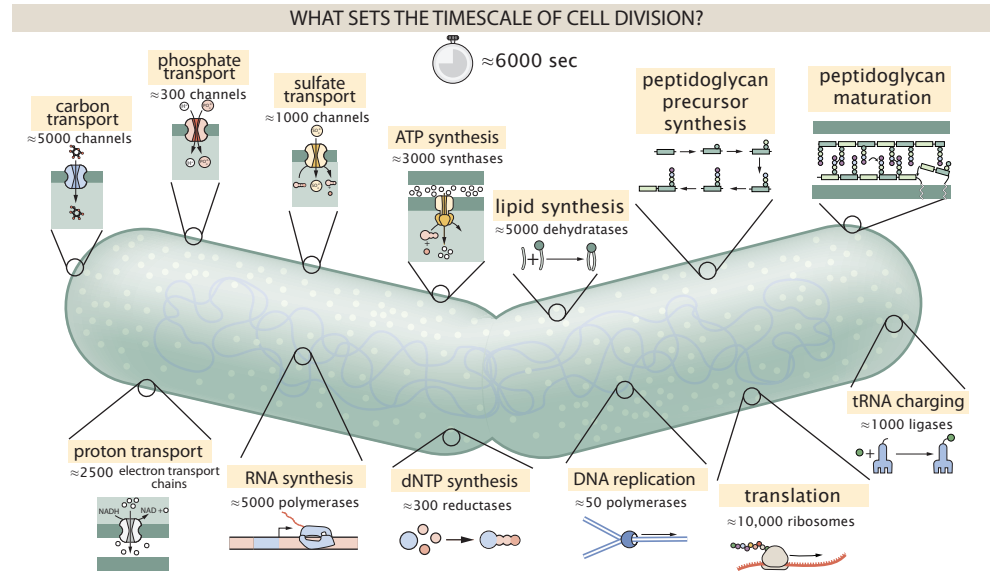


**Figure 1. Transport and synthesis processes necessary for cell division.** We consider an array of processes necessary for a cell to double its molecular components. Such processes include the transport of carbon across the cell membrane, the production of ATP, and fundamental processes of the central dogma namely RNA, DNA, and protein synthesis. A schematic of each synthetic or transport category is shown with an approximate measure of the complex abundance at a growth rate of 0.5 per hour. In this work, we consider a standard bacterial division time of  $\approx 5000$  sec.

92 engage in a dialogue between back-of-the-envelope estimates for the numbers of transporters  
 93 needed to facilitate these chemical stoichiometries and the experimental proteomic measurements  
 94 of the biological reality. Such an approach provides the opportunity to test if our biological knowl-  
 95 edge is sufficient to understand the scale at which these complexes are produced. Specifically, we  
 96 will make these estimates considering a modest doubling time of 5000 s, a growth rate of  $\approx 0.5 \text{ hr}^{-1}$ ,  
 97 the range in which the majority of the experimental measurements reside.

### 98 Carbon Transport

99 We begin with the most abundant element by mass, carbon. Using  $\approx 0.3 \text{ pg}$  as the typical *E. coli*  
 100 dry mass (BNID: 103904, *Milo et al. (2010)*), we estimate that  $\approx 10^{10}$  carbon atoms must be brought  
 101 into the cell in order to double all of the carbon-containing molecules (*Figure 2(A, top)*). Typical  
 102 laboratory growth conditions, such as those explored in the aforementioned proteomic data sets,  
 103 provide carbon as a single class of sugar such as glucose, galactose, or xylose to name a few. *E.*  
 104 *coli* has evolved myriad mechanisms by which these sugars can be transported across the cell  
 105 membrane. One such mechanism of transport is via the PTS system which is a highly modular  
 106 system capable of transporting a diverse range of sugars (*Escalante et al., 2012*). The glucose-  
 107 specific component of this system transports  $\approx 200$  glucose molecules per second per channel  
 108 (BNID: 114686, *Milo et al. (2010)*). Making the assumption that this is a typical sugar transport rate,  
 109 coupled with the need to transport  $10^{10}$  carbon atoms, we arrive at the conclusion that on the order  
 110 of 1,000 transporters must be expressed in order to bring in enough carbon atoms to divide in  
 111 6,000 s, diagrammed in the top panel of *Figure 2(A)*. This estimate, along with the observed average  
 112 number of carbohydrate transporters present in the proteomic data sets (*Schmidt et al., 2016*;  
 113 *Peebo et al., 2015; Valgepea et al., 2013; Li et al., 2014*), is shown in *Figure 2(A)*. While we estimate  
 114 1,000 transporters are needed, the data reveals that at a division time of  $\approx 5000$  s there is nearly  
 115 a ten-fold excess of transporters. Furthermore, the data illustrates that the average number of  
 116 carbohydrate transporters present is largely-growth rate independent.

117 The estimate presented in *Figure 2(A)* neglects any specifics of the regulation of carbon transport

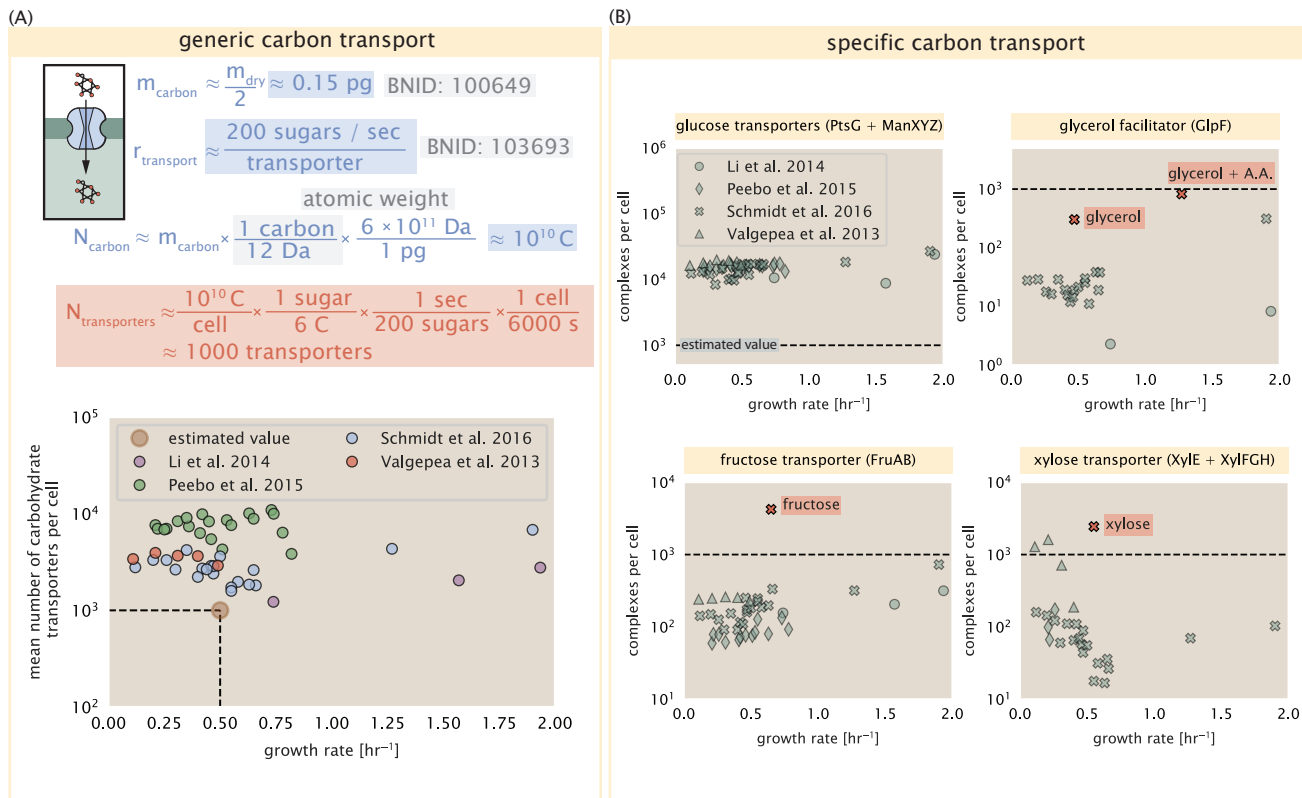


**Figure 2. The abundance of carbon transport systems across growth rates.** (A) A simple estimate for the minimum number of generic carbohydrate transport systems (top) assumes  $\approx 10^{10}$  C are needed to complete division, each transported sugar contains  $\approx 6$  C, and each transporter conducts sugar molecules at a rate of  $\approx 200$  per second. Bottom plot shows the estimated number of transporters needed at a growth rate of  $\approx 0.5$  per hr (light-brown point and dashed lines). Colored points correspond to the mean number of carbohydrate transporters for different growth conditions across different published datasets. (B) The abundance of various specific carbon transport systems plotted as a function of the population growth rate. Red points and red-highlighted text indicate conditions in which the only source of carbon in the growth medium induces expression of the transport system.

118 system and presents a data-averaged view of how many carbohydrate transporters are present  
 119 on average. Using the diverse array of growth conditions explored in the proteomic data sets, we  
 120 can explore how individual carbon transport systems depend on the population growth rate. In  
 121 **Figure 2(B)**, we show the total number of carbohydrate transporters specific to different carbon  
 122 sources. A striking observation, shown in the top-left plot of **Figure 2(B)**, is the constancy in the  
 123 expression of the glucose-specific transport systems (the PtsG enzyme of the PTS system and the  
 124 glucose-transporting ManXYZ complex). Additionally, we note that the total number of glucose-  
 125 specific transporters is tightly distributed  $\approx 10^4$  per cell, an order of magnitude beyond the estimate  
 126 shown in **Figure 2(A)**. This illustrates that *E. coli* maintains a substantial number of complexes  
 127 present for transporting glucose which is known to be the preferential carbon source (**Monod, 1947**;  
 128 **Liu et al., 2005; Aidelberg et al., 2014**).

129 It is now understood that a large number of metabolic operons are regulated with dual-input  
 130 logic gates that are only expressed when glucose concentrations are low (mediated by cyclic-AMP  
 131 receptor protein CRP) and the concentration of other carbon sources are elevated (**Gama-Castro**  
 132 **et al., 2016; Zhang et al., 2014b**). A famed example of such dual-input regulatory logic is in the  
 133 regulation of the *lac* operon which is only natively activated in the absence of glucose and the  
 134 presence of allolactose, an intermediate in lactose metabolism (**Jacob and Monod, 1961**), though we  
 135 now know of many other such examples (**Ireland et al., 2020; Gama-Castro et al., 2016; Belliveau**  
 136 **et al., 2018**). This illustrates that once glucose is depleted from the environment, cells have a means  
 137 to dramatically increase the abundance of the specific transporter needed to digest the next sugar  
 138 that is present. Several examples of induced expression of specific carbon-source transporters  
 139 are shown in **Figure 2(B)**. Points colored in red (labeled by red text-boxes) correspond to growth  
 140 conditions in which the specific carbon source (glycerol, xylose, or fructose) is present. These  
 141 plots show that, in the absence of the particular carbon source, expression of the transporters is  
 142 maintained on the order of  $\sim 10^2$  per cell. However, when induced, the transporters become highly-  
 143 expressed and are present on the order of  $\sim 10^4$  per cell, which exceeds the generic estimate given  
 144 in **Figure 2(A)**. Together, this generic estimation and the specific examples of induced expression  
 145 suggest that transport of carbon across the cell membrane, while critical for growth, is not the  
 146 rate-limiting step of cell division.

147 In the context of speeding up growth, one additional limitation is the fact that the cell's inner  
 148 membrane is occupied by a multitude of other membrane proteins. Considering a rule-of-thumb  
 149 for the surface area of *E. coli* of about  $6 \mu\text{m}^2$  (BNID: 101792, **Milo et al. (2010)**), we expect an  
 150 areal density for 1,000 transporters to be approximately 200 transporters/ $\mu\text{m}^2$ . For a glucose  
 151 transporter occupying about  $50 \text{ nm}^2/\text{dimer}$ , this amounts to about only 1 percent of the total inner  
 152 membrane (**Szenk et al., 2017**). In addition, bacterial cell membranes typically have densities of  
 153  $10^5$  proteins/ $\mu\text{m}^2$  (**Phillips, 2018**), implying that the cell could accommodate more transporters if it  
 154 were rate limiting.

### 155 Phosphorus and Sulfur Transport

156 We now turn our attention towards other essential elements, namely phosphorus and sulfur.  
 157 Phosphorus is critical to the cellular energy economy in the form of high-energy phosphodiester  
 158 bonds making up DNA, RNA, and the NTP energy pool as well as playing a critical role in the post-  
 159 translational modification of proteins and defining the polar-heads of lipids. In total, phosphorus  
 160 makes up  $\approx 3\%$  of the cellular dry mass which in typical experimental conditions is in the form of  
 161 inorganic phosphate. The cell membrane has remarkably low permeability to this highly-charged  
 162 and critical molecule, therefore requiring the expression of active transport systems. In *E. coli*, the  
 163 proton electrochemical gradient across the inner membrane is leveraged to transport inorganic  
 164 phosphate into the cell (**Rosenberg et al., 1977**). Proton-solute symporters are widespread in *E. coli*  
 165 (**Ramos and Kaback, 1977; Booth et al., 1979**) and can have rapid transport rates of 50 molecules  
 166 per second for sugars and other solutes (BNID: 103159; 111777, **Milo et al. (2010)**). In *E. coli* the PitA  
 167 phosphate transport system has been shown to very tightly coupled with the proton electrochemical

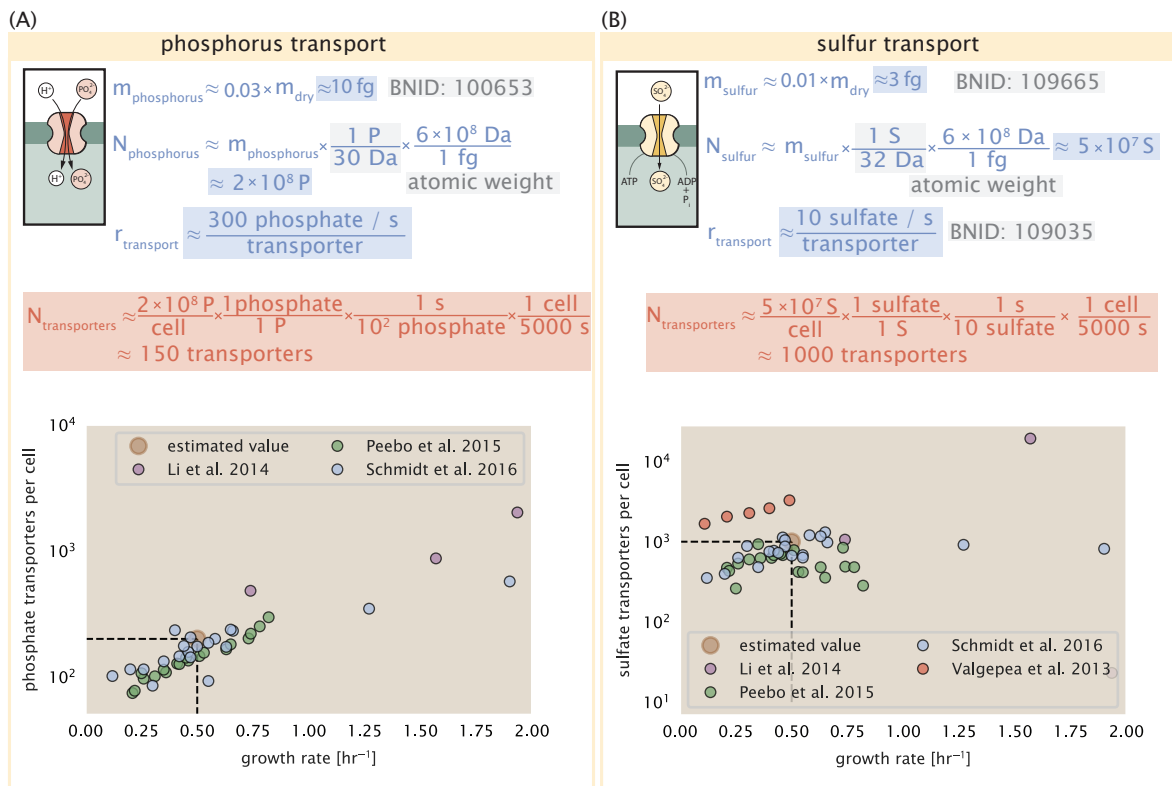


**Figure 3. Estimates and measurements of phosphate and sulfate transport systems as a function of growth rate.** (A) Estimate for the number of PitA phosphate transport systems needed to maintain a 3% phosphorus *E. coli* dry mass. Points in plot correspond to the total number of PitA transporters per cell. (B) Estimate of the number of CysUWA complexes necessary to maintain a 1% sulfur *E. coli* dry mass. Points in plot correspond to average number of CysUWA transporter complexes that can be formed given the transporter stoichiometry [CysA]<sub>2</sub>[CysU][CysW][Sbp/CysP].

gradient with a 1:1 proton:phosphate stoichiometric ratio (*Harris et al., 2001; Feist et al., 2007*). Illustrated in *Figure 3(A)*, we can estimate that  $\approx 300$  phosphate transporters are necessary to maintain an  $\approx 3\%$  dry mass with a 6,000 s division time. This estimate is again satisfied when we examine the observed copy numbers of PitA in proteomic data sets (plot in *Figure 3(A)*). While our estimate is very much in line with the observed numbers, we emphasize that this is likely a slight overestimate of the number of transporters needed as there are other phosphorous scavenging systems, such as the ATP-dependent phosphate transporter Pst system which we have neglected.

Satisfied that there are a sufficient number of phosphate transporters present in the cell, we now turn to sulfur transport as another potentially rate limiting process. Similar to phosphate, sulfate is highly-charged and not particularly membrane permeable, requiring active transport. While there exists a H<sup>+</sup>/sulfate symporter in *E. coli*, it is in relatively low abundance and is not well characterized (*Zhang et al., 2014a*). Sulfate is predominantly acquired via the ATP-dependent ABC transporter CysUWA system which also plays an important role in selenium transport (*Sekowska et al., 2000; Sirko et al., 1995*). While specific kinetic details of this transport system are not readily available, generic ATP transport systems in prokaryotes transport on the order of 1 to 10 molecules per second (BNID: 109035, *Milo et al. (2010)*). Combining this generic transport rate, measurement of sulfur comprising 1% of dry mass, and a 6,000 second division time yields an estimate of  $\approx 1000$  CysUWA complexes per cell (*Figure 3(B)*). Once again, this estimate is in notable agreement with proteomic data sets, suggesting that there are sufficient transporters present to acquire the necessary sulfur. In a similar spirit of our estimate of phosphorus transport, we emphasize that this is likely an overestimate of the number of necessary transporters as we have neglected other sulfur scavenging systems that are in lower abundance.

190 **Nitrogen Transport**

191 Finally, we turn to nitrogen transport as the last remaining transport system highlighted in **Figure 1**.  
 192 Unlike phosphate, sulfate, and various sugar molecules, nitrogen in the form of ammonia can readily  
 193 diffuse across the cell membrane and has a permeability on par with water ( $\approx 10^5$  nm/s, BNID:110824  
 194 **Milo et al. (2010)**). In particularly nitrogen-poor conditions, *E. coli* expresses a transporter (AmtB)  
 195 which appears to aid in nitrogen assimilation, though the mechanism and kinetic details of transport  
 196 is still a matter of debate (**van Heeswijk et al., 2013; Khademi et al., 2004**). Beyond ammonia,  
 197 another plentiful source of nitrogen come in the form of glutamate, which has its own complex  
 198 metabolism and scavenging pathways. However, nitrogen is plentiful in the growth conditions  
 199 examined in this work, permitting us to neglect nitrogen transport as a potential rate limiting  
 200 process in cell division.

201 **Function of the Central Dogma**

202 Up to this point, we have considered a variety of transport and biosynthetic processes that are  
 203 critical to acquiring and generating new cell mass. While there are of course many other metabolic  
 204 processes we could consider and perform estimates of (such as the components of fermentative  
 205 versus aerobic respiration), we now turn our focus to some of the most central processes which  
 206 must be undertaken irrespective of the growth conditions – the processes of the central dogma.

207 **DNA**

208 Most bacteria (including *E. coli*) harbor a single, circular chromosome and can have extra-chromosomal  
 209 plasmids  $\sim 100$  kbp in length. We will focus our quantitative thinking solely on the chromosome  
 210 of *E. coli* which harbors  $\approx 5000$  genes and  $\approx 5 \times 10^6$  base pairs. To successfully divide and produce  
 211 viable progeny, this chromosome must be faithfully replicated and segregated into each nascent  
 212 cell. We again rely on the near century of literature in molecular biology to provide some insight  
 213 towards the rates and mechanics of the replicative feat as well as the production of the replication  
 214 starting materials, dNTPs.

215 **dNTP synthesis**

216 We begin our exploration of the DNA replicative processes by examining the production of the  
 217 deoxyribonucleotide triphosphates (dNTPs). The four major dNTPS (dATP, dTTP, dCTP, and dGTP)  
 218 are synthesized *de novo* in separate pathways, requiring different building blocks. However, a  
 219 critical step present in all dNTP synthesis pathways is the conversion from ribonucleotide to  
 220 deoxyribonucleotide via the removal of the 3' hydroxyl group of the ribose ring (**Rudd et al., 2016**).  
 221 This reaction is mediated by a class of enzymes termed ribonucleotide reductases, of  
 222 which *E. coli* possesses two aerobically active complexes (termed I and II) and a single anaerobically  
 223 active enzyme. Due to their peculiar formation of a radical intermediate, these enzymes have  
 224 received much biochemical, kinetic, and structural characterization. One such work (**Ge et al., 2003**)  
 225 performed a detailed *in vitro* measurement of the steady-state kinetic rates of these complexes,  
 226 revealing a turnover rate of  $\approx 10$  per second.

227 Considering this reaction (mediated by the ribonucleotide reductase complexes I and II) is  
 228 central to synthesis of all dNTPS, it is reasonable to consider the abundance of these complexes  
 229 as a measure of the total dNTP production in *E. coli*. Illustrated schematically in **Figure 4 (A)**, we  
 230 consider the fact that to replicate the cell's genome, on the order of  $\approx 10^7$  dNTPs must be  
 231 synthesized. Assuming a production rate of 10 per second per ribonucleotide reductase complex  
 232 and a cell division time of 6000 seconds, we arrive at an estimate of  $\approx 150$  complexes are needed  
 233 per cell. As shown in the bottom panel of **Figure 4 (A)**, this estimate agrees with the experimental  
 234 measurements of these complexes abundances within  $\approx 1/2$  an order of magnitude.

235 Recent work has revealed that during replication, the ribonucleotide reductase complexes  
 236 coalesce to form discrete foci colocalized with the DNA replisome complex (**Sánchez-Romero et al.,**

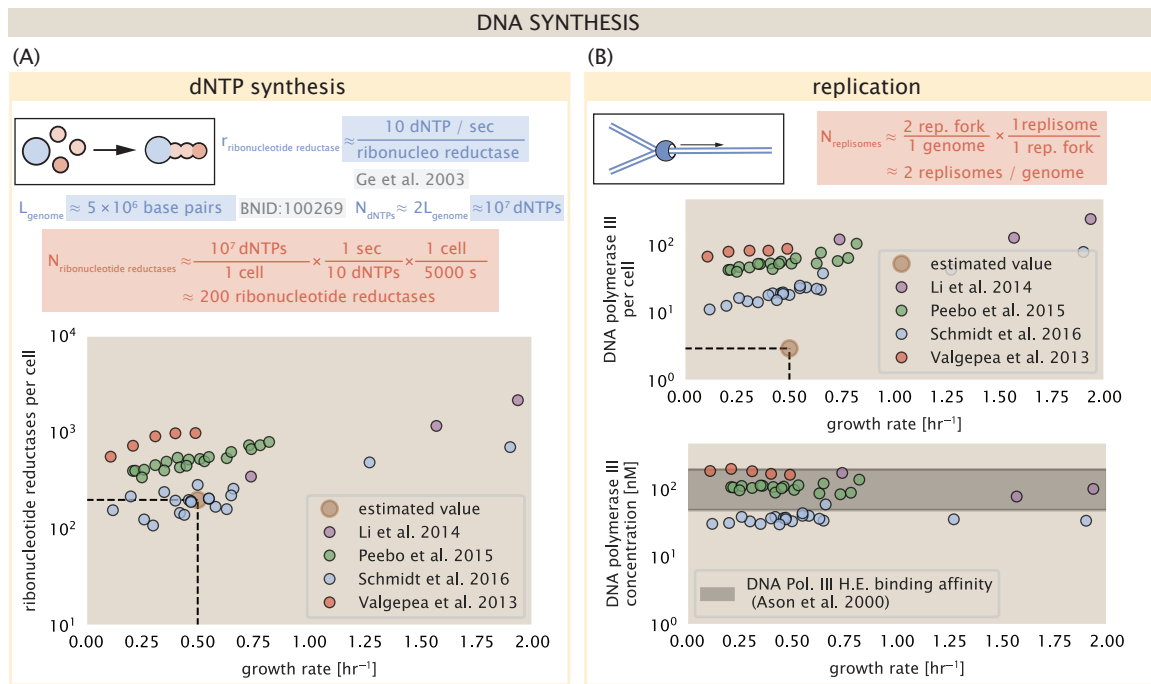


**Figure 4. Complex abundance estimates for dNTP synthesis and DNA replication.** (A) Estimate of the number of ribonucleotide reductase enzymes needed to facilitate the synthesis of  $\approx 10^7$  dNTPs over the course of a 6000 second generation time. Points in the plot correspond to the total number of ribonucleotide reductase I ( $[NrdA]_2[NrdB]_2$ ) and ribonucleotide reductase II ( $[NrdE]_2[NrdF]_2$ ) complexes. (B) An estimate for the minimum number of DNA polymerase holoenzyme complexes needed to facilitate replication of a single genome. Points in the top plot correspond to the total number of DNA polymerase III holoenzyme complexes ( $[DnaE]_3[DnaQ]_3[HolE]_3[DnaX]_5[HolB][HolA][DnaN]_4[HolC]_4[Hold]_4$ ) per cell. Bottom plot shows the effective concentration of DNA polymerase III holoenzyme given cell volumes calculated from the growth rate as in *Si et al. (2019)*.

237 **2011).** This is particularly pronounced in environments where growth is slow, indicating that spatial  
238 organization and regulation of the activity of the complexes plays an important role.

### 239 DNA Replication

240 We now turn our focus towards the process of integration of the dNTP building blocks into the  
241 replicated chromosome strand via the DNA polymerase enzymes. Replication of bacterial chromo-  
242 somes is initiated at a single region of the chromosome termed the *oriC* locus at which a pair of  
243 DNA polymerases bind and begin their high-fidelity replication of the genome in opposite directions.  
244 Assuming equivalence between the two replication forks, this means that the two DNA polymerase  
245 complexes (termed replisomes) meet at the midway point of the circular chromosome termed  
246 the *ter* locus. This division of labor means The kinetics of the five types of DNA polymerases  
247 (I – V) have been intensely studied, revealing that DNA polymerase III performs the high fidelity  
248 processive replication of the genome with the other "accessory" polymerases playing auxiliary roles  
249 (*Fijalkowska et al., 2012*). *In vitro* measurements have shown that DNA Polymerase III copies DNA  
250 at a rate of  $\approx 600$  nucleotides per second (BNID: 104120, *Milo et al. (2010)*). Therefore, to replicate a  
251 single chromosome, two DNA polymerases replicating at their maximal rate would copy the entire  
252 genome in  $\approx 4000$  s. Thus, with a division time of 6000 s (our "typical" growth rate for the purposes  
253 of this work), there is sufficient time for a pair of DNA polymerase III complexes to replicate the  
254 entire genome. However, this estimate implies that 4000 s would be the upper-limit time scale for  
255 bacterial division which is at odds with the familiar  $\approx 1500$  s doubling time of *E. coli* in rich medium.

256 It is known well known that *E. coli* can parallelize its DNA replication such that multiple chromo-  
257 somes are being replicated at once. Recent work (*Si et al., 2017*) has shown that the replicative  
258 timescale of cell division can be massively parallelized where *E. coli* can have on the order of 10 - 12

replication forks at a given time. Thus, even in rapidly growing cultures, only a few polymerases ( $\approx 10$ ) are needed to replicate the chromosome. However, as shown in **Figure 4(B)**, DNA polymerase III is nearly an order of magnitude more abundant. This discrepancy can be understood when considering the binding affinities. The DNA polymerase III complex is highly processive, facilitated by a strong affinity of the complex to the DNA. *In vitro* biochemical characterization has quantified the  $K_D$  of DNA polymerase III holoenzyme to single-stranded and double-stranded DNA to be 50 and 200 nM, respectively (*Ason et al., 2000*). The bottom plot in **Figure 4(B)** shows that the concentration of the DNA polymerase III across all data sets and growth conditions is within this range. Thus, while the copy number of the DNA polymerase III is in excess of the strict number required to replicate the genome, the copy number is tuned such that the concentration is approximately equal to the dissociation constant to the DNA. While the processes regulating the initiation of DNA replication are complex and involve more than just the holoenzyme, these data indicate that the kinetics of replication rather than the explicit copy number of the DNA polymerase III holoenzyme is the more relevant feature of DNA replication to consider.

### RNA Synthesis

With the machinery governing the replication of the genome accounted for, we now turn our attention to the next stage of the central dogma – the transcription of DNA to form RNA. We primarily consider three major groupings of RNA, namely the RNA associated with ribosomes (rRNA), the RNA encoding the amino-acid sequence of proteins (mRNA), and the RNA which links codon sequence to amino-acid identity during translation (tRNA). Despite the varied function of these RNA species, they share a commonality in that they are transcribed from DNA via the action of RNA polymerase. In the coming paragraphs, we will consider the synthesis of RNA as a rate limiting step in bacterial division by estimating how many RNA polymerases must be present to synthesize all necessary rRNA, mRNA, and tRNA.

#### rRNA

We begin with an estimation of the number of RNA polymerases needed to synthesize the rRNA that serve as catalytic and structural elements of the ribosome. Each ribosome contains three rRNA molecules of lengths 120, 1542, and 2904 nucleotides (BNID: 108093, *Milo et al. (2010)*), meaning each ribosome contains  $\approx 4500$  nucleotides. As the *E. coli* RNA polymerase transcribes DNA to RNA at a rate of  $\approx 40$  nucleotides per second (BNID: 101904, *Milo et al. (2010)*), it takes a single RNA polymerase  $\approx 100$  s to synthesize the RNA needed to form a single functional ribosome. Therefore, in a 5000 s division time, a single RNA polymerase transcribing rRNA at a time would result in only  $\approx 50$  functional ribosomal rRNA units – far below the observed number of  $\approx 10^4$  ribosomes per cell.

Of course, there can be more than one RNA polymerase transcribing the rRNA genes at any given time. To elucidate the *maximum* number of rRNA units that can be synthesized given a single copy of each rRNA gene, we will consider a hypothesis in which the rRNA operon is completely tiled with RNA polymerase. *In vivo* measurements of the kinetics of rRNA transcription have revealed that RNA polymerases are loaded onto the promoter of an rRNA gene at a rate of  $\approx 1$  per second (BNID: 111997; 102362, *Milo et al. (2010)*). If RNA polymerases are being constantly loaded on to the rRNA genes at this rate, then we can make the approximation that  $\approx 1$  functional rRNA unit is synthesized per second. With a 5000 second division time, this hypothesis leads to a maximal value of 5000 functional rRNA units, still undershooting the observed number of  $10^4$  ribosomes per cell.

*E. coli* has evolved a clever mechanism to surpass this kinetic limit for the rate of rRNA production. Rather than having only one copy of each rRNA gene, *E. coli* has seven copies of the operon (BNID: 100352, *Milo et al. (2010)*) four of which are localized directly adjacent to the origin of replication (*Birnbaum and Kaplan, 1971*). As fast growth requires that multiple copies are being synthesized simultaneously, this means that the total number of rRNA genes can be on the order of  $\approx 10 - 70$  at moderate to fast growth rates (*Stevenson and Schmidt, 2004*). Using our standard time scale of a 5000 second division time, we can make the lower-bound estimate that the typical cell will have

308 7 copies of the rRNA operon. Synthesizing one functional rRNA unit per second per operon, a total  
 309 of  $4 \times 10^4$  rRNA units can be synthesized, comfortably above the observed number of ribosomes  
 310 per cell.

311 How many RNA polymerases are then needed to constantly transcribe 7 copies of the rRNA  
 312 genes? We approach this estimate by considering the maximum number of RNA polymerases can be  
 313 tiling the rRNA genes with a loading rate of 1 per second and a transcription rate of 40 nucleotides  
 314 per second. Considering that a RNA polymerase has a physical footprint of approximately 40  
 315 nucleotides (BNID: 107873, *Milo et al. (2010)*), we can state that there is  $\approx 1$  RNA polymerase per  
 316 80 nucleotides. With a total length of  $\approx 4500$  nucleotides per operon and 7 operons per cell, the  
 317 maximum number of RNA polymerases that can be transcribing rRNA at any given time is  $\approx 400$ . As  
 318 we will see in the coming sections, the synthesis of rRNA is the dominant requirement of the RNA  
 319 polymerase pool.

### 320 mRNA

321 To form a functional protein, all protein coding genes must first be transcribed from DNA to form  
 322 an mRNA molecule. While each protein requires an mRNA blueprint, many copies of the protein  
 323 can be synthesized from a single mRNA. Factors such as strength of the ribosomal binding site,  
 324 mRNA stability, and rare codon usage frequency dictate the number of proteins that can be made  
 325 from a single mRNA, with yields ranging from  $10^1$  to  $10^4$  (BNID: 104186; 100196; 106254, *Milo et al.*  
 326 (*2010*)). Computing the geometric mean of this range yields  $\approx 1000$  proteins synthesized per mRNA,  
 327 a value that agrees with experimental measurements of the number of proteins per cell ( $\approx 3 \times 10^6$ ,  
 328 BNID: 100088, *Milo et al. (2010)*) and total number of mRNA per cell ( $\approx 3 \times 10^3$ , BNID:100064, *Milo*  
 329 *et al. (2010)*).

330 This estimation captures the *steady state* mRNA copy number, meaning that at any given time,  
 331 there will exist approximately 3000 unique mRNA molecules. To determine the *total* number of  
 332 mRNA that need to be synthesized over the cell's lifetime, we must consider degradation of the  
 333 mRNA. In most bacteria, mRNAs are rather unstable with life times on the order of several minutes  
 334 (BNID: 104324; 106253; 111927; 111998, *Milo et al. (2010)*). For convenience, we will assume that  
 335 the typical mRNA in our cell of interest has a typical lifetime of  $\approx 300$  seconds. Using this value, we  
 336 can determine the total mRNA production rate to maintain a steady-state copy number of 3000  
 337 mRNA per cell. While we direct the reader to the appendix for a more detailed discussion of mRNA  
 338 transcriptional dynamics, we state here that the total mRNA production rate must be on the order  
 339 of  $\approx 15$  mRNA made every second. In *E. coli*, the average protein is  $\approx 300$  amino acids in length  
 340 (BNID: 108986; *Milo et al. (2010)*), meaning that the corresponding mRNA is  $\approx 900$  nucleotides  
 341 which we will further approximate to be  $\approx 1000$  nucleotides given non-protein coding regions of the  
 342 mRNA present on the 5' and 3' ends. This means that the cell must have enough RNA polymerase  
 343 molecules about to sustain a transcription rate of  $\approx 1.5 \times 10^4$  nucleotides per second. Knowing that  
 344 a single RNA polymerase polymerizes RNA at a clip of 40 nucleotides per second, we arrive at a  
 345 comfortable estimate of  $\approx 250$  RNA polymerase complexes needed to satisfy the mRNA demands  
 346 of the cell. It is worth noting that this number is approximately half of that required to synthesize  
 347 enough rRNA, as we saw in the previous section. We find this to be a striking result as these 250  
 348 RNA polymerase molecules are responsible for the transcription of the  $\approx 4000$  protein coding genes  
 349 which are not ribosome associated.

### 350 tRNA

351 The final class of RNA molecules worthy of quantitative consideration is the the pool of tRNAs  
 352 used during translation to map codon sequence to amino acid identity. Unlike mRNA or rRNA,  
 353 each individual tRNA is remarkably short, ranging from 70 to 95 nucleotides each (BNID: 109645;  
 354 102340, *Milo et al. (2010)*). What they lack in length, they make up for in abundance. There are  
 355 approximately  $\approx 3000$  tRNA molecules present for each of the 20 amino acids (BNID: 105280, *Milo*  
 356 *et al. (2010)*), although the precise copy number is dependent on the identity of the ligated amino

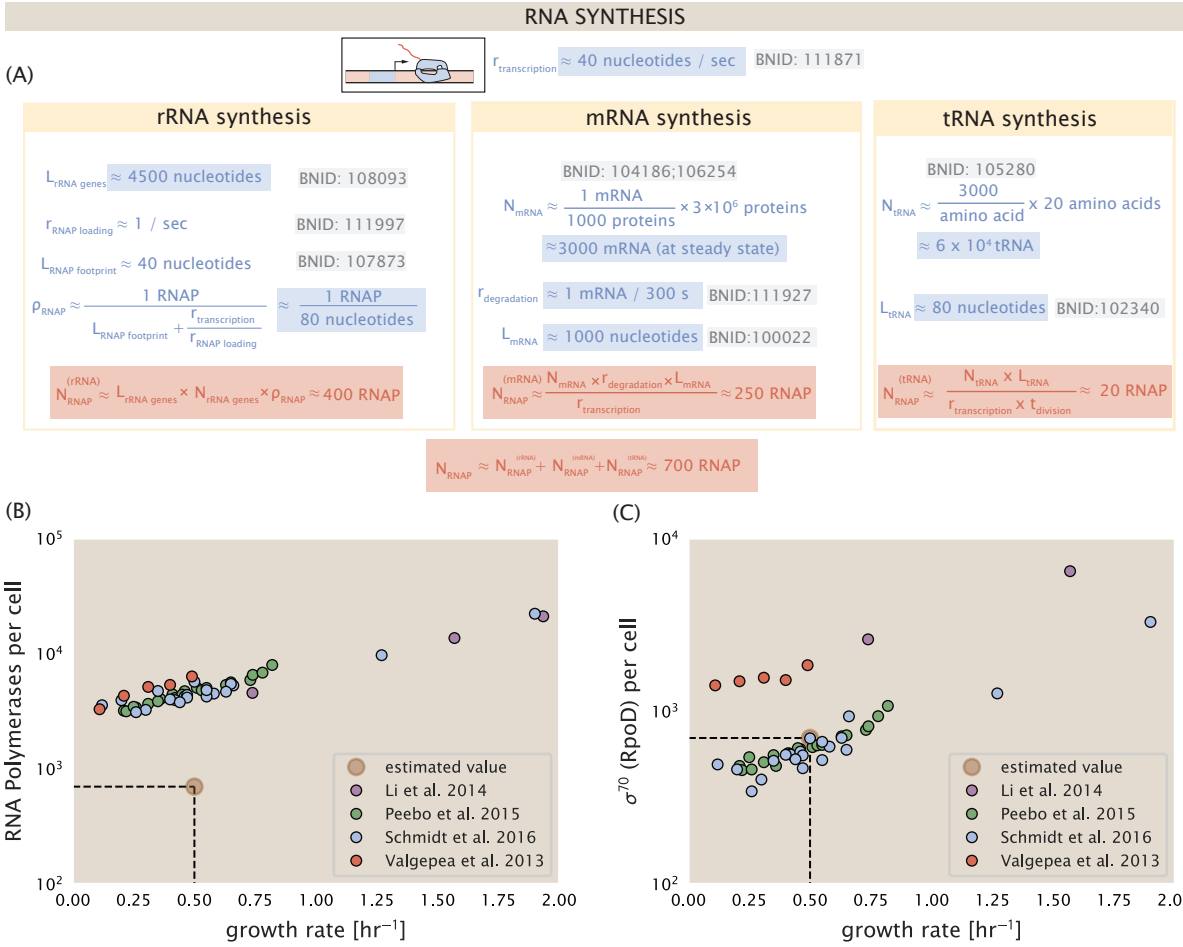


**Figure 5. Estimation of the RNA polymerase demand and comparison with experimental data.** (A) Estimations for the number of RNA polymerase needed to synthesize sufficient quantities of rRNA, mRNA, and tRNA from left to right, respectively. Bionumber Identifiers (BNIDs) are provided for key quantities used in the estimates. (B) The RNA polymerase core enzyme copy number as a function of growth rate. Colored points correspond to the average number RNA polymerase core enzymes that could be formed given a subunit stoichiometry of [RpoA]<sub>2</sub>[RpoC][RpoB]. (C) The abundance of  $\sigma^{70}$  (RpoD) as a function of growth rate. Estimated value for the number of RNAP is shown in (B) and (C) as a translucent brown point at a growth rate of  $0.5 \text{ hr}^{-1}$ .

acid. Using these values, we make the estimate that  $\approx 5 \times 10^6$  nucleotides are sequestered in tRNA per cell. Unlike mRNA, tRNA is remarkably stable with typical lifetimes *in vivo* on the order of  $\approx 48$  hours (Abelson et al., 1974; Svenningsen et al., 2017) – well beyond the timescale of division. Once again using our rule-of-thumb for the rate of transcription to be 40 nucleotides per second and assuming a division time of  $\approx 5000$  seconds, we arrive at an estimate of  $\approx 20$  RNA polymerases to synthesize enough tRNA. This requirement pales in comparison to the number of polymerases needed to generate the rRNA and mRNA pools and can be neglected as a significant transcriptional burden.

#### 365 RNA Polymerase and $\sigma$ -factor Abundance

366 These estimates, summarized in **Figure 5 (A)**, reveal that synthesis of rRNA and mRNA are the  
 367 dominant forces dictating the number of RNA polymerases needed per cell. For completeness, we  
 368 can use our estimates of  $\approx 400$ ,  $250$ , and  $20$  RNA polymerases needed to synthesize the required  
 369 number of rRNAs, mRNAs, and tRNAs, respectively, to state that the typical cell needs to maintain  
 370 a pool of  $\approx 700$  RNA polymerases. As is revealed in **Figure 5 (B)**, this estimate is about an order  
 371 of magnitude below the observed number of RNA polymerase complexes per cell ( $\approx 5000$  -  $7000$ ).

372 This disagreement between the estimated number of transcriptionally active RNA polymerases  
 373 and these observations jibes with recent literature revealing that  $\approx 80\%$  of RNA polymerases in  
 374 *E. coli* are not transcriptionally active (**Patrick et al., 2015**). This leads us to consider other factors  
 375 intimately involved in transcription may set the scale of this curious balance.

376 One such factor we can consider is the influence of  $\sigma$ -factors, namely  $\sigma^{70}$  (RpoD) which is the  
 377 dominant "general-purpose"  $\sigma$ -factor in *E. coli*. While initially thought of as being solely involved  
 378 in transcriptional initiation, the past two decades of single-molecule work has revealed a more  
 379 multipurpose role for  $\sigma^{70}$  including facilitating transcriptional elongation (**Kapanidis et al., 2005**;  
 380 **Goldman et al., 2015; Perdue and Roberts, 2011; Mooney and Landick, 2003; Mooney et al., 2005**).  
 381 **Figure 5** (B) is suggestive of such a role as the number of  $\sigma^{70}$  proteins per cell is in close agreement  
 382 with our estimate of the number of transcriptional complexes needed. In the appendix and  
 383 supplemental figure XXX [GC: format number later], the slope of the  $\sigma^{70}$  abundance as a factor  
 384 of the growth rate can be very accurately estimated by factoring in a) the growth-rate dependent  
 385 size of the proteome and b) the rRNA gene dosage resulting from parallelized replication of the  
 386 chromosome.

387 While these estimates and comparison with experimental data reveal an interesting dynamic at  
 388 play between the transcriptional demand and copy numbers of the corresponding machinery, these  
 389 findings illustrate that transcription cannot be the rate limiting step in bacterial division. **Figure 5**  
 390 (A) reveals that the availability of RNA polymerase is not a limiting factor for cell division as there is  
 391  $\sim 10$ -fold more complexes than needed. Furthermore, if more transcriptional activity was needed  
 392 to satisfy the cellular requirements, more  $\sigma^{70}$ -factors could be expressed to utilize a larger fraction  
 393 of the RNA polymerase pool.

### 394 Protein synthesis

395 Lastly, we turn our attention to the process of translation. So far in our various estimates there  
 396 has been little to suggest any apparent limit to how fast a bacterium might divide under steady-  
 397 state growth. Even in our examples of *E. coli* grown rapidly under different carbohydrate sources  
 398 (**Figure 2(B)**), cells are able to utilize less preferred carbon sources by inducing the expression of  
 399 additional membrane transporters and enzymes. [Maybe go into Hwa style resource allocation with  
 400 references added]. In this respect, gross overexpression of a protein can lead to a reduction of the  
 401 growth rate.

402 We can determine the translation-limited growth rate by noting that the total number of peptide  
 403 bonds created as the cell doubles  $N_{aa}$  will be given by,  $\tau \cdot r_t \cdot R$ . Here,  $\tau$  refers to the doubling time of  
 404 the cell under steady-state growth,  $r_t$  is the maximum translation rate, and  $R$  is the average number  
 405 of ribosomes in the cell. With the growth rate related to the cell doubling time by  $\lambda = \ln(2)/\tau$ , we  
 406 can write the translation-limited growth rate as,

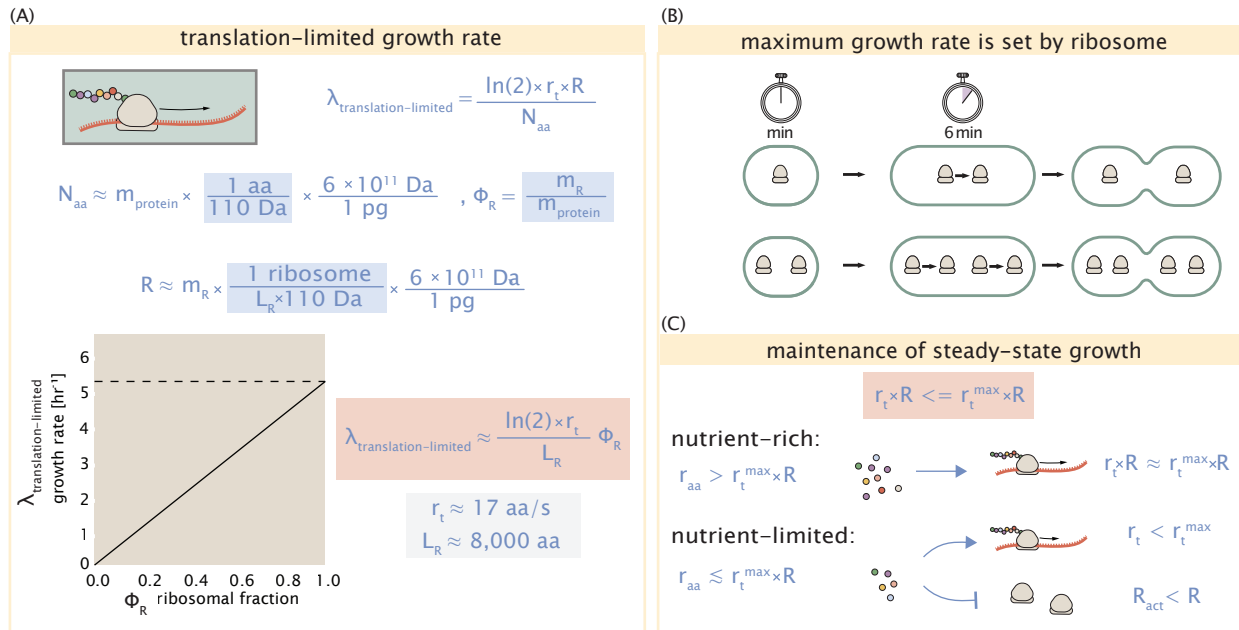
$$\lambda_{\text{translation-limited}} = \frac{\ln(2) \cdot r_t \cdot R}{N_{aa}}. \quad (1)$$

407 Alternatively, since  $N_{aa}$  is related to the total protein mass through the molecular weight of each  
 408 protein, we can also consider the growth rate in terms of ribosomal mass fraction. This calculation  
 409 is shown in **Figure 6(A)**. This allows us to rewrite the growth rate as,

$$\lambda_{\text{translation-limited}} \approx \frac{\ln(2) \cdot r_t}{L_R} \Phi_R, \quad (2)$$

410 where  $L_R$  is the total length in amino acids that make up a ribosome, and  $\Phi_R$  is the ribosomal mass  
 411 fraction. This is plotted as a function of ribosomal fraction  $\Phi_R$  in **Figure 6(A)**, with a translation rate  
 412  $r_t = 17\text{aa/s}$  and  $L_R = 105\text{aa}$ , which corresponds to the length in amino acids for all ribosomal subunits  
 413 of the 50S and 30S complexes and elongation factor required for translation.

414 Perhaps the first thing to notice is that there is a maximum growth rate at about  $\lambda \approx 6\text{hr}^{-1}$ , or  
 415 doubling time of about 7 minutes. This maximum growth rate can be viewed as an inherent speed

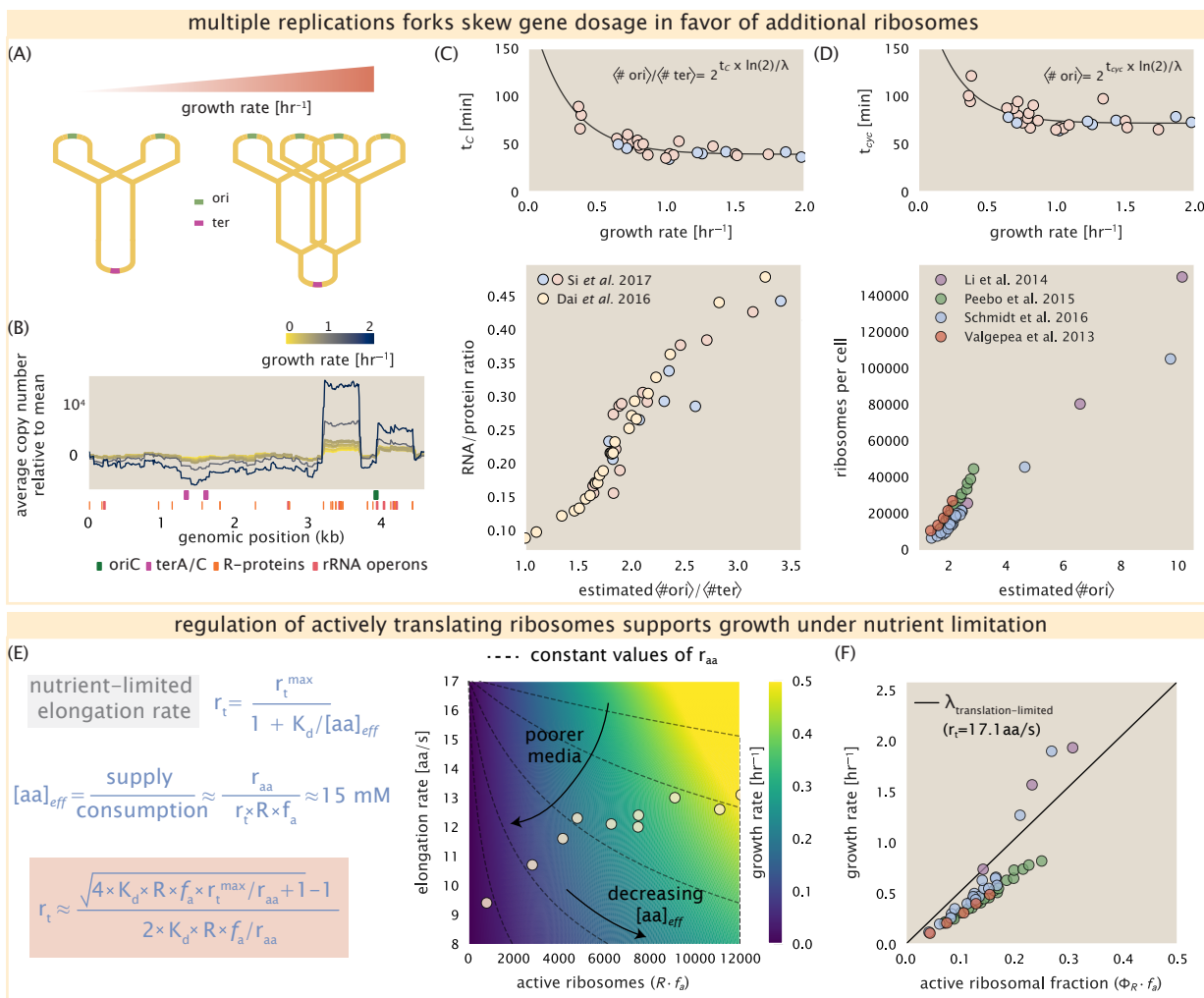


**Figure 6. Translation-limited growth rate.** (A) Here we consider the translation-limited growth as a function of ribosomal fraction. By mass balance, the time required to double the entire proteome ( $N_{\text{aa}} / r_t$ ) sets the translation-limited growth rate,  $\lambda_{\text{translation-limited}}$ . Here  $N_{\text{aa}}$  is effectively the number of peptide bonds that must be translated,  $r_t$  is the translation elongation rate, and  $R$  is the number of ribosomes. This can also be re-written in terms of the ribosomal mass fraction  $\Phi_R = m_R / m_{\text{protein}}$ , where  $m_R$  is the total ribosomal mass and  $m_{\text{protein}}$  is the mass of all proteins in the cell.  $L_R$  refers to the summed length of the ribosome in amino acids.  $\lambda_{\text{translation-limited}}$  is plotted as a function of  $\Phi_R$  (solid line). (B) The dashed line in part (A) identifies a maximum growth rate that is set by the ribosome. Specifically, this growth rate corresponds to the time required to translate an entire ribosome,  $L_R / r_t$ . This is a result that is independent of the number of ribosomes in the cell as shown schematically here. (C)

416 limit due to the need for the cell to double the cell's entire ribosomal mass. Interestingly, this limit  
 417 is independent of the absolute number of ribosomes, but rather is simply given by time to translate  
 418 an entire ribosome,  $L_R / r_t$ . As shown in **Figure 6(B)**, we can reconcile this with the observation  
 419 that in order to double the average number of ribosomes, each ribosome must produce a second  
 420 ribosome. This is a process that cannot be parallelized further.

421 Since a cell consists of more than just ribosomes, we can see that for  $\Phi_R$  in the range of about  
 422 0.1 - 0.3, the maximum growth rate is in line with experimentally reported growth rates around 0.5 -  
 423 2  $\text{hr}^{-1}$ . Here we have implicitly assumed that translation proceeds randomly, without preference  
 424 between ribosomal or non-ribosomal mRNA, which appears reasonable. Importantly, in order  
 425 for a cell to scale this limit set by  $\Phi_R$  the cell must increase its ribosomal abundance, either by  
 426 synthesizing more ribosomes or reducing the fraction of non-ribosomal proteins.

427 One additional point to note is that across different species of bacteria, cells do not decrease  
 428 their ribosomal abundance to zero in the limit of poorer nutrient condition [CITE?]. Indeed, some  
 429 organisms appear to have constant ribosomal abundance irrespective of their growth rate [NB:  
 430 ask Griffin and figure out what organism this is]. From the perspective of a bacterium dealing  
 431 with uncertain nutrient conditions, there is likely a benefit for the cell to maintain some relative  
 432 fraction of ribosomes to support rapid growth as nutrient conditions improve. In addition, given  
 433 their massive size at about 850 kDa, they may play an as-yet fully understood role as a crowding  
 434 agent in cellular function *Delarue et al. (2018); Soler-Bistué et al. (2020)*. If we consider a scenario  
 435 where nutrient conditions become poorer and poorer, there must be a regime where the cell has  
 436 more ribosomes than it can utilize. While this perhaps suggests less import to the process of  
 437 translation, it is important to recognize that in order for a cell to maintain steady-state growth, the  
 438 cell's translation capacity must be mitigated. Otherwise, ribosomes will deplete their supply of  
 439 amino acids and this will bring translation and cell growth to a halt (**Figure 6(C)**). We will consider  
 440 the consequences of this in the case of *E. coli* next.

**Figure 7. . (A) (B) (C).**

#### 441     Multiple replication forks provide one strategy to support faster growth.

442     We now turn to our proteomic data from *E. coli* and plot the ribosomal fraction as a function of  
 443     reported growth rate. Here we find that the ribosomal fraction always increases with growth rate.  
 444     This is consistent with the behavior expected for *E. coli*, and an observation of intense study related  
 445     to the so-called nutrient-limited growth law. In terms of absolute ribosomal abundance, we find  
 446     that cells increase both their quantity and cellular concentration at faster growth.

447     One feature of *E. coli*, as well as other bacteria like *B. subtilis*, is the ability to begin replication of  
 448     multiple copies of its genome during a single cell cycle. This is achieved through multiple initiation  
 449     forks and nested DNA replication. [need to refer to work from Jun lab here!! - under adder  
 450     mechanism, the cell appears to add a certain cell mass in proportion to its number of origins]. We  
 451     find that the ribosome copy number increases in proportion to the expected number of origins.  
 452     The process of nested DNA replication will lead to a bias in gene dosage for genes closer to the  
 453     origin of replication () Importantly, ribosomal protein and rRNA genes are closer to the origin of  
 454     replication **Scholz et al. (2019)** and this provides a natural way for *E. coli* to bias the proportion of  
 455     ribosomes at faster growth without the advent of additional gene regulation strategies. Given that  
 456     ribosomal genes in *E. coli* appear to be transcribed at their maximal rate at fast growth rates [cite??],  
 457     increasing ribosomal copy number through increased gene dosage represents a creative approach  
 458     for the cell to grow faster without gross down-regulation of non-ribosomal genes.

## 459      References

- 460      Abelson, H., Johnson, L., Penman, S., and Green, H. (1974). Changes in RNA in relation to growth of the fibroblast:  
461      II. The lifetime of mRNA, rRNA, and tRNA in resting and growing cells. *Cell*, 1(4):161–165.
- 462      Aidelberg, G., Towbin, B. D., Rothschild, D., Dekel, E., Bren, A., and Alon, U. (2014). Hierarchy of non-glucose  
463      sugars in *Escherichia coli*. *BMC Systems Biology*, 8(1):133.
- 464      Antonenko, Y. N., Pohl, P., and Denisov, G. A. (1997). Permeation of ammonia across bilayer lipid membranes  
465      studied by ammonium ion selective microelectrodes. *Biophysical Journal*, 72(5):2187–2195.
- 466      Ason, B., Bertram, J. G., Hingorani, M. M., Beechem, J. M., O'Donnell, M., Goodman, M. F., and Bloom, L. B.  
467      (2000). A Model for *Escherichia coli* DNA Polymerase III Holoenzyme Assembly at Primer/Template Ends:  
468      DNA Triggers A Change In Binding Specificity of the  $\gamma$  Complex Clamp Loader. *Journal of Biological Chemistry*,  
469      275(4):3006–3015.
- 470      Assentoft, M., Kaptan, S., Schneider, H.-P., Deitmer, J. W., de Groot, B. L., and MacAulay, N. (2016). Aquaporin 4  
471      as a NH3 Channel. *Journal of Biological Chemistry*, 291(36):19184–19195.
- 472      Bauer, S. and Ziv, E. (1976). Dense growth of aerobic bacteria in a bench-scale fermentor. *Biotechnology and  
473      Bioengineering*, 18(1):81–94. \_eprint: <https://onlinelibrary.wiley.com/doi/10.1002/bit.260180107>.
- 474      Belliveau, N. M., Barnes, S. L., Ireland, W. T., Jones, D. L., Sweredoski, M. J., Moradian, A., Hess, S., Kinney, J. B., and  
475      Phillips, R. (2018). Systematic approach for dissecting the molecular mechanisms of transcriptional regulation  
476      in bacteria. *Proceedings of the National Academy of Sciences*, 115(21):E4796–E4805.
- 477      Birnbaum, L. S. and Kaplan, S. (1971). Localization of a Portion of the Ribosomal RNA Genes in *Escherichia coli*.  
478      *Proceedings of the National Academy of Sciences*, 68(5):925–929.
- 479      Booth, I. R., Mitchell, W. J., and Hamilton, W. A. (1979). Quantitative analysis of proton-linked transport systems.  
480      The lactose permease of *Escherichia coli*. *Biochemical Journal*, 182(3):687–696.
- 481      Delarue, M., Brittingham, G. P., Pfeffer, S., Surovtsev, I. V., Pinglay, S., Kennedy, K. J., Schaffer, M., Gutierrez,  
482      J. I., Sang, D., Poterewicz, G., Chung, J. K., Plitzko, J. M., Groves, J. T., Jacobs-Wagner, C., Engel, B. D., and Holt,  
483      L. J. (2018). mTORC1 Controls Phase Separation and the Biophysical Properties of the Cytoplasm by Tuning  
484      Crowding. *Cell*, 174(2):338–349.e20.
- 485      Escalante, A., Salinas Cervantes, A., Gosset, G., and Bolívar, F. (2012). Current knowledge of the *Escherichia coli*  
486      phosphoenolpyruvate–carbohydrate phosphotransferase system: Peculiarities of regulation and impact on  
487      growth and product formation. *Applied Microbiology and Biotechnology*, 94(6):1483–1494.
- 488      Feist, A. M., Henry, C. S., Reed, J. L., Krummenacker, M., Joyce, A. R., Karp, P. D., Broadbelt, L. J., Hatzimanikatis, V.,  
489      and Palsson, B. Ø. (2007). A genome-scale metabolic reconstruction for *Escherichia coli* K-12 MG1655 that  
490      accounts for 1260 ORFs and thermodynamic information. *Molecular Systems Biology*, 3(1):121.
- 491      Fijalkowska, I. J., Schaaper, R. M., and Jonczyk, P. (2012). DNA replication fidelity in *Escherichia coli*: A multi-DNA  
492      polymerase affair. *FEMS Microbiology Reviews*, 36(6):1105–1121.
- 493      Gama-Castro, S., Salgado, H., Santos-Zavaleta, A., Ledezma-Tejeida, D., Muñiz-Rascado, L., García-Sotelo, J. S.,  
494      Alquicira-Hernández, K., Martínez-Flores, I., Pannier, L., Castro-Mondragón, J. A., Medina-Rivera, A., Solano-Lira,  
495      H., Bonavides-Martínez, C., Pérez-Rueda, E., Alquicira-Hernández, S., Porrón-Sotelo, L., López-Fuentes, A.,  
496      Hernández-Koutoucheva, A., Moral-Chávez, V. D., Rinaldi, F., and Collado-Vides, J. (2016). RegulonDB version  
497      9.0: High-level integration of gene regulation, coexpression, motif clustering and beyond. *Nucleic Acids  
498      Research*, 44(D1):D133–D143.
- 499      Ge, J., Yu, G., Ator, M. A., and Stubbe, J. (2003). Pre-Steady-State and Steady-State Kinetic Analysis of *E. coli* Class I  
500      Ribonucleotide Reductase. *Biochemistry*, 42(34):10071–10083.
- 501      Goldman, S. R., Nair, N. U., Wells, C. D., Nickels, B. E., and Hochschild, A. (2015). The primary  $\sigma$  factor in *Escherichia  
502      coli* can access the transcription elongation complex from solution *in vivo*. *eLife*, 4:e10514.
- 503      Harris, R. M., Webb, D. C., Howitt, S. M., and Cox, G. B. (2001). Characterization of PitA and PitB from *Escherichia  
504      coli*. *Journal of Bacteriology*, 183(17):5008–5014.
- 505      Heldal, M., Norland, S., and Tumyr, O. (1985). X-ray microanalytic method for measurement of dry matter and  
506      elemental content of individual bacteria. *Applied and Environmental Microbiology*, 50(5):1251–1257.

- 507 Ireland, W. T., Beeler, S. M., Flores-Bautista, E., Belliveau, N. M., Sweredoski, M. J., Moradian, A., Kinney, J. B., and  
 508 Phillips, R. (2020). Deciphering the regulatory genome of *Escherichia coli*, one hundred promoters at a time.  
 509 *bioRxiv*.
- 510 Jacob, F. and Monod, J. (1961). Genetic regulatory mechanisms in the synthesis of proteins. *Journal of Molecular  
 511 Biology*, 3(3):318–356.
- 512 Jun, S., Si, F., Pugatch, R., and Scott, M. (2018). Fundamental principles in bacterial physiology - history, recent  
 513 progress, and the future with focus on cell size control: A review. *Reports on Progress in Physics*, 81(5):056601.
- 514 Kapanidis, A. N., Margeat, E., Laurence, T. A., Doose, S., Ho, S. O., Mukhopadhyay, J., Kortkhonja, E., Mekler, V.,  
 515 Ebright, R. H., and Weiss, S. (2005). Retention of Transcription Initiation Factor  $\Sigma$ 70 in Transcription Elongation:  
 516 Single-Molecule Analysis. *Molecular Cell*, 20(3):347–356.
- 517 Khademi, S., O'Connell, J., Remis, J., Robles-Colmenares, Y., Miercke, L. J. W., and Stroud, R. M. (2004). Mechanism  
 518 of Ammonia Transport by Amt/MEP/Rh: Structure of AmtB at 1.35 Å. *Science*, 305(5690):1587–1594.
- 519 Li, G.-W., Burkhardt, D., Gross, C., and Weissman, J. S. (2014). Quantifying absolute protein synthesis rates  
 520 reveals principles underlying allocation of cellular resources. *Cell*, 157(3):624–635.
- 521 Liu, M., Durfee, T., Cabrera, J. E., Zhao, K., Jin, D. J., and Blattner, F. R. (2005). Global Transcriptional Programs  
 522 Reveal a Carbon Source Foraging Strategy by *Escherichia coli*. *Journal of Biological Chemistry*, 280(16):15921–  
 523 15927.
- 524 Milo, R., Jorgensen, P., Moran, U., Weber, G., and Springer, M. (2010). BioNumbers—the database of key numbers  
 525 in molecular and cell biology. *Nucleic Acids Research*, 38(suppl\_1):D750–D753.
- 526 Monod, J. (1947). The phenomenon of enzymatic adaptation and its bearings on problems of genetics and  
 527 cellular differentiation. *Growth Symposium*, 9:223–289.
- 528 Mooney, R. A., Darst, S. A., and Landick, R. (2005). Sigma and RNA Polymerase: An On-Again, Off-Again  
 529 Relationship? *Molecular Cell*, 20(3):335–345.
- 530 Mooney, R. A. and Landick, R. (2003). Tethering  $\Sigma$ 70 to RNA polymerase reveals high *in vivo* activity of  $\sigma$  factors  
 531 and  $\Sigma$ 70-dependent pausing at promoter-distal locations. *Genes & Development*, 17(22):2839–2851.
- 532 Neidhardt, F. C., Ingraham, J., and Schaechter, M. (1991). *Physiology of the Bacterial Cell - A Molecular Approach*,  
 533 volume 1. Elsevier.
- 534 Patrick, M., Dennis, P. P., Ehrenberg, M., and Bremer, H. (2015). Free RNA polymerase in *Escherichia coli*. *Biochimie*,  
 535 119:80–91.
- 536 Peebo, K., Valgepea, K., Maser, A., Nahku, R., Adamberg, K., and Vilu, R. (2015). Proteome reallocation in  
 537 *Escherichia coli* with increasing specific growth rate. *Molecular BioSystems*, 11(4):1184–1193.
- 538 Perdue, S. A. and Roberts, J. W. (2011).  $\sigma^{70}$ -dependent Transcription Pausing in *Escherichia coli*. *Journal of  
 539 Molecular Biology*, 412(5):782–792.
- 540 Phillips, R. (2018). Membranes by the Numbers. In *Physics of Biological Membranes*, pages 73–105. Springer,  
 541 Cham, Cham.
- 542 Ramos, S. and Kaback, H. R. (1977). The relation between the electrochemical proton gradient and active  
 543 transport in *Escherichia coli* membrane vesicles. *Biochemistry*, 16(5):854–859.
- 544 Rosenberg, H., Gerdes, R. G., and Chegwidden, K. (1977). Two systems for the uptake of phosphate in *Escherichia coli*.  
 545 *Journal of Bacteriology*, 131(2):505–511.
- 546 Rudd, S. G., Valerie, N. C. K., and Helleday, T. (2016). Pathways controlling dNTP pools to maintain genome  
 547 stability. *DNA Repair*, 44:193–204.
- 548 Sánchez-Romero, M. A., Molina, F., and Jiménez-Sánchez, A. (2011). Organization of ribonucleoside diphosphate  
 549 reductase during multifork chromosome replication in *Escherichia coli*. *Microbiology*, 157(8):2220–2225.
- 550 Schmidt, A., Kochanowski, K., Vedelaar, S., Ahrné, E., Volkmer, B., Callipo, L., Knoops, K., Bauer, M., Aebersold,  
 551 R., and Heinemann, M. (2016). The quantitative and condition-dependent *Escherichia coli* proteome. *Nature  
 552 Biotechnology*, 34(1):104–110.

- 553 Scholz, S. A., Diao, R., Wolfe, M. B., Fivenson, E. M., Lin, X. N., and Freddolino, P. L. (2019). High-Resolution  
 554 Mapping of the Escherichia coli Chromosome Reveals Positions of High and Low Transcription. *Cell Systems*,  
 555 8(3):212–225.e9.
- 556 Scott, M., Gunderson, C. W., Mateescu, E. M., Zhang, Z., and Hwa, T. (2010). Interdependence of cell growth and  
 557 gene expression: origins and consequences. *Science*, 330(6007):1099–1102.
- 558 Sekowska, A., Kung, H.-F., and Danchin, A. (2000). Sulfur Metabolism in Escherichia coli and Related Bacteria:  
 559 Facts and Fiction. *Journal of Molecular Microbiology and Biotechnology*, 2(2):34.
- 560 Si, F., Le Treut, G., Sauls, J. T., Vadia, S., Levin, P. A., and Jun, S. (2019). Mechanistic Origin of Cell-Size Control and  
 561 Homeostasis in Bacteria. *Current Biology*, 29(11):1760–1770.e7.
- 562 Si, F., Li, D., Cox, S. E., Sauls, J. T., Azizi, O., Sou, C., Schwartz, A. B., Erickstad, M. J., Jun, Y., Li, X., and Jun, S. (2017).  
 563 Invariance of Initiation Mass and Predictability of Cell Size in Escherichia coli. *Current Biology*, 27(9):1278–1287.
- 564 Sirko, A., Zatyka, M., Sadowy, E., and Hulanicka, D. (1995). Sulfate and thiosulfate transport in Escherichia coli  
 565 K-12: Evidence for a functional overlapping of sulfate- and thiosulfate-binding proteins. *Journal of Bacteriology*,  
 566 177(14):4134–4136.
- 567 Soler-Bistué, A., Aguilar-Pierlé, S., García-Garcéa, M., Val, M.-E., Sismeiro, O., Varet, H., Sieira, R., Krin, E.,  
 568 Skovgaard, O., Comerci, D. J., Eduardo P. C. Rocha, and Mazel, D. (2020). Macromolecular crowding links  
 569 ribosomal protein gene dosage to growth rate in *Vibrio cholerae*. *BMC Biology*, 18(1):1–18.
- 570 Stasi, R., Neves, H. I., and Spira, B. (2019). Phosphate uptake by the phosphonate transport system PhnCDE.  
 571 *BMC Microbiology*, 19.
- 572 Stevenson, B. S. and Schmidt, T. M. (2004). Life History Implications of rRNA Gene Copy Number in *Escherichia coli*. *Applied and Environmental Microbiology*, 70(11):6670–6677.
- 573 Svenningsen, S. L., Kongstad, M., Stenum, T. S. n., Muñoz-Gómez, A. J., and Sørensen, M. A. (2017). Transfer RNA  
 574 is highly unstable during early amino acid starvation in *Escherichia coli*. *Nucleic Acids Research*, 45(2):793–804.
- 575 Szenk, M., Dill, K. A., and de Graff, A. M. R. (2017). Why Do Fast-Growing Bacteria Enter Overflow Metabolism?  
 576 Testing the Membrane Real Estate Hypothesis. *Cell Systems*, 5(2):95–104.
- 577 Taymaz-Nikerel, H., Borujeni, A. E., Verheijen, P. J. T., Heijnen, J. J., and van Gulik, W. M.  
 578 (2010). Genome-derived minimal metabolic models for *Escherichia coli* MG1655 with estimated  
 579 in vivo respiratory ATP stoichiometry. *Biotechnology and Bioengineering*, 107(2):369–381. \_eprint:  
 580 <https://onlinelibrary.wiley.com/doi/pdf/10.1002/bit.22802>.
- 581 Valgepea, K., Adamberg, K., Seiman, A., and Vilu, R. (2013). *Escherichia coli* achieves faster growth by increasing  
 582 catalytic and translation rates of proteins. *Molecular BioSystems*, 9(9):2344.
- 583 van Heeswijk, W. C., Westerhoff, H. V., and Boogerd, F. C. (2013). Nitrogen Assimilation in *Escherichia coli*: Putting  
 584 Molecular Data into a Systems Perspective. *Microbiology and Molecular Biology Reviews*, 77(4):628–695.
- 585 Willsky, G. R., Bennett, R. L., and Malamy, M. H. (1973). Inorganic Phosphate Transport in *Escherichia coli*:  
 586 Involvement of Two Genes Which Play a Role in Alkaline Phosphatase Regulation. *Journal of Bacteriology*,  
 587 113(2):529–539.
- 588 Zhang, L., Jiang, W., Nan, J., Almqvist, J., and Huang, Y. (2014a). The *Escherichia coli* CysZ is a pH dependent  
 589 sulfate transporter that can be inhibited by sulfite. *Biochimica et Biophysica Acta (BBA) - Biomembranes*,  
 590 1838(7):1809–1816.
- 591 Zhang, Z., Aboulwafa, M., and Saier, M. H. (2014b). Regulation of crp gene expression by the catabolite  
 592 repressor/activator, cra, in *Escherichia coli*. *Journal of Molecular Microbiology and Biotechnology*, 24(3):135–141.